THE JOURNAL OF PHYSICAL CHEMISTRY Letters

Letter

pubs.acs.org/JPCL

Heterovalent Dopant Incorporation for Bandgap and Type Engineering of Perovskite Crystals

Ahmed L. Abdelhady,[†,‡,⊥] Makhsud I. Saidaminov,[†,⊥] Banavoth Murali,[†] Valerio Adinolfi,[§] Oleksandr Voznyy,[§] Khabiboulakh Katsiev,[∥] Erkki Alarousu,[†] Riccardo Comin,[§] Ibrahim Dursun,[†] Lutfan Sinatra,[†] Edward H. Sargent,[§] Omar F. Mohammed,[*,†] and Osman M. Bakr[*,†]

[†]Division of Physical Sciences and Engineering, Solar and Photovoltaics Engineering Research Center, King Abdullah University of Science and Technology (KAUST), Thuwal 23955-6900, Kingdom of Saudi Arabia

[‡]Department of Chemistry, Faculty of Science, Mansoura University, Mansoura, 35516, Egypt

[§]Department of Electrical and Computer Engineering, University of Toronto, Toronto, Ontario M5S 3G4, Canada

[∥]SABIC Corporate Research and Innovation Center, King Abdullah University of Science and Technology (KAUST), Thuwal, 23955-6900, Kingdom of Saudi Arabia

Supporting Information

ABSTRACT: Controllable doping of semiconductors is a fundamental technological requirement for electronic and optoelectronic devices. As intrinsic semiconductors, hybrid perovskites have so far been a phenomenal success in photovoltaics. The inability to dope these materials heterovalently (or aliovalently) has greatly limited their wider utilizations in electronics. Here we show an efficient in situ chemical route that achieves the controlled incorporation of trivalent cations (Bi^{3+}, Au^{3+}, or In^{3+}) by exploiting the retrograde solubility behavior of perovskites. We term the new method dopant incorporation in the retrograde regime. We achieve Bi^{3+} incorporation that leads to bandgap tuning (~300 meV), 10^4 fold enhancement in electrical conductivity, and a change in the sign of majority charge carriers from positive to negative. This work demonstrates the successful incorporation of dopants into perovskite crystals while preserving the host lattice structure, opening new avenues to tailor the electronic and optoelectronic properties of this rapidly emerging class of solution-processed semiconductors.

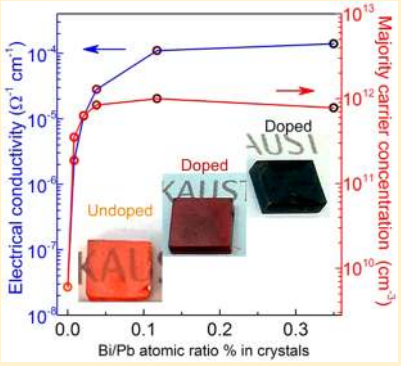

Doping of semiconductors is fundamental to modern electronic and optoelectronic devices.[1] Doping enables manipulation of both the optical[2,3] and the electrical properties of semiconductors—keys to device functionality.[1]

The properties of the doped semiconductors strongly depend on the electronic levels introduced by the dopants.[1,4−6] Upon increasing the dopant concentration, the discrete impurity levels in the band gap of the host semiconductor evolve into an impurity band that can overlap with the conduction/valence band in n-/p-type semiconductors, respectively,[1,4,7] resulting in bandgap narrowing (BGN).[1,5−7] In semiconductors, the bandgap is integral to device architecture and expected performance, such as governing the limits of power conversion efficiency (PCE) in solar cells.[5] In the case of semiconductors, incorporating a high concentration of dopants, band tails appear as a consequence of the large disorder in the distribution of the density of states,[4,7] and these can be useful in applications such as nonlinear optical switching.[7,8]

Hybrid trihalide perovskites, especially $MAPbX_3$ (MA = $CH_3NH_3^+$, X = Br^- or I^-), have seen intensive investigation,[9−16] particularly in the context of photovoltaic applications following early studies beginning in 2009.[17] In only a few years, the field has witnessed a remarkable increase in the PCE of polycrystalline thin film perovskite-based solar cells, recently reaching certified efficiencies of 20.1%.[18] The incorporation of dopants offers a route to tailor hybrid perovskites and endow them with new properties.

To date, $MAPbX_3$ has primarily been doped using elements that are isovalent with the anion (I^-/Cl^-)[19−22] or with the metal cation Pb^{2+}/M^{2+} (M^{2+} = Sn^{2+}, Sr^{2+}, Cd^{2+} or Ca^{2+}).[23] This limits dopants' capacity to impact the sign or concentration of the majority charge carriers. By contrast, heterovalent doping in semiconductors has a propensity to switch the sign of majority charge carrier from n- to p-type or vice versa and, if established in hybrid perovskites, could permit the fabrication of devices based on a p−n perovskite homojunction with minimal lattice mismatch. In addition, incorporation of heterovalent cations into the hybrid trihalide perovskite could potentially extend their spectral range to longer wavelengths. However, despite the promised benefits, the complete absence of reports on the heterovalent doping of hybrid trihalide perovskite polycrystalline films and, more importantly, crystals reflects the challenge

Received: December 2, 2015
Accepted: January 2, 2016
Published: January 2, 2016

DOI: 10.1021/acs.jpclett.5b02681
J. Phys. Chem. Lett. 2016, 7, 295−301

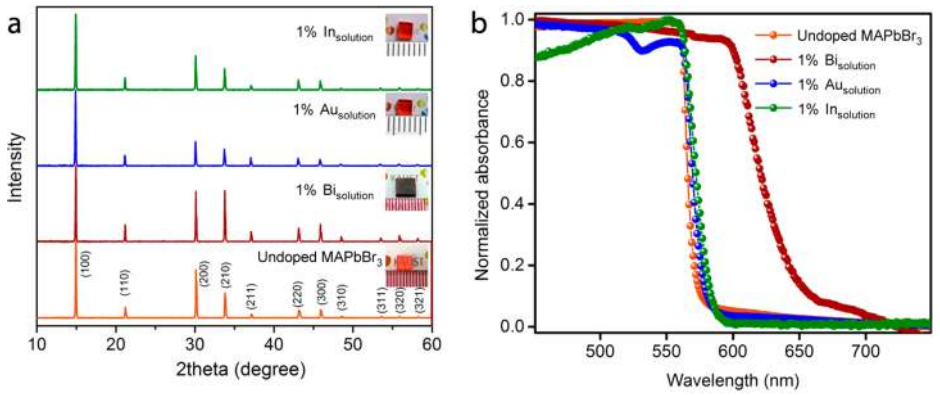

Figure 1. (a) Powder XRD of ground $MAPbBr_3$ and doped crystals prepared from solutions containing 1% dopant precursor. The inset above each XRD pattern shows the picture of the corresponding as-grown crystal. (b) Steady-state absorption spectra of $MAPbBr_3$ crystals with and without cation doping.

of incorporating differently charged cations into perovskites. This challenge derives from the demanding requirement that incorporated dopants satisfy both octahedral and tolerance factors while maintaining the same underlying crystal structure.

It is well documented that the introduction of Cl^- into perovskite precursors solutions can significantly alter the crystallinity, morphology, and grain size of the obtained thin films, the combined effects of which appreciably impact device performance.[20,21,24,25] Given this combination of mechanisms, it has been difficult to isolate the specific role of the chloride additive on polycrystalline thin film properties.

Studying single crystals, which are not conflated by grain boundary and morphological effects, offers to put the focus on the role of dopants on the underlying properties of the material. There are, however, a number of constraints and challenges to classical crystal growth techniques associated with devising a general heterovalent doping approach of $MAPbX_3$ crystals. For example, employing antisolvent vapor-assisted crystallization[26] requires the choice of a solvent−antisolvent combination that is suitable for all precursors. Also, crystal growth by cooling from a saturated solution[27] occurs at temperatures that are likely too low to dissociate the dopant from its precursor state. Moreover, in each of these methods, crystallization occurs at a very slow rate, approaching the near-equilibrium conditions that militate against the incorporation of impurities into the host lattice.

We reasoned that the in situ incorporation of a dopant might be feasible using the inverse temperature solubility regime, a regime peculiar to hybrid perovskites. In this regime, crystallization occurs at astonishingly rapid rates at moderately elevated temperatures.[28,29] The approach we explore herein, dopant incorporation in the retrograde regime (DIRR), offers advantages that overcome many of the shortcomings of other methods: it requires the use of only a single solvent; its rapidity provides a higher probability of incorporation of impurities; and its use of moderately elevated temperatures enhances the chances of dissociation of precursor-solvent complexes,[29] making the impurities more readily available for incorporation.

Additional consideration, beyond the suitable choice of reaction conditions, must be given to designing a heterovalent doping strategy. We tried various trivalent cations, focusing on Bi^{3+} (isoelectronic with Pb^{2+}, i.e. having the same electronic structure), Au^{3+}, or In^{3+}, which fit into the perovskite tolerance factor.[30] Tolerance factors for Bi^{3+}, Au^{3+}, and In^{3+} were calculated to be 0.889, 0.946, and 0.963, respectively. These values fall within the range (0.75−1.00) reported to allow the formation of perovskites.[30]

As a result of the development of the DIRR process, we report herein an efficient in situ solution-processed method for the synthesis of heterovalent doped hybrid perovskite crystals. The successful incorporation of trivalent dopants (Bi^{3+}, Au^3+, or In^{3+}) into $MAPbBr_3$ crystals demonstrates the flexibility of the perovskite structure to host a number of different heterovalent cations. Our studies also reveal the considerable influence of dopants on the properties of the underlying semiconductor. In particular, we achieved a high concentration of Bi^{3+} reaching $\sim 10^{19}$ cm^{-3}, although the active carrier concentration was ~7 orders of magnitude less than this (but still ~100 fold greater than the undoped crystals) and we also showed conclusively that variation in bismuth concentration in the feed crystallization solution directly impacts both optical and electronic properties of $MAPbBr_3$. The introduction of Bi^{3+} as a dopant resulted in significant bandgap narrowing (~300 meV), an enhancement of charge carrier concentration, a 3 to 4 orders of magnitude increase in conductivity, and sign switching of the majority carriers. Based on our results, Bi may be of particular interest in ongoing efforts to narrow the bandgap of hybrid perovskites, including iodide perovskite crystals, in the direction of the 1.0−1.3 eV range optimal for single junction solar cells.[31]

We implemented in situ incorporation of dopants by adding a mixture of trivalent (Bi^{3+}, Au^{3+}, In^{3+}) bromide salts and MABr into a crystallization solution containing a mixture of $PbBr_2$ and MABr in DMF, and then heating to the required temperature (synthesis is described in detail in the Methods section in the Supporting Information). After 3 h, bulk crystals—entirely lacking grain boundaries (Figure S1, Supporting Information)—of parallelepiped shape (the same as undoped $MAPbBr_3$) were formed. We observed a color change, from orange to deep red, in Bi-doped crystals, but not for other dopants (inset in Figure 1a). In the case of Au-doped crystals, the dark color of the solution (which is due to the presence of $AuBr_3$) became much lighter (Figure S2, Supporting Information). This color fading could be attributed to either the incorporation of the Au^{3+} ions in the perovskite crystal or to the reduction of Au^{3+} to Au^+.

The exact dopant content in the crystals grown by DIRR was quantified using inductively coupled plasma optical emission spectrometry (ICP-OES). The dopant/Pb atomic ratio % in crystals synthesized from a feed solution containing 1%

DOI: 10.1021/acs.jpclett.5b02681
J. Phys. Chem. Lett. 2016, 7, 295−301

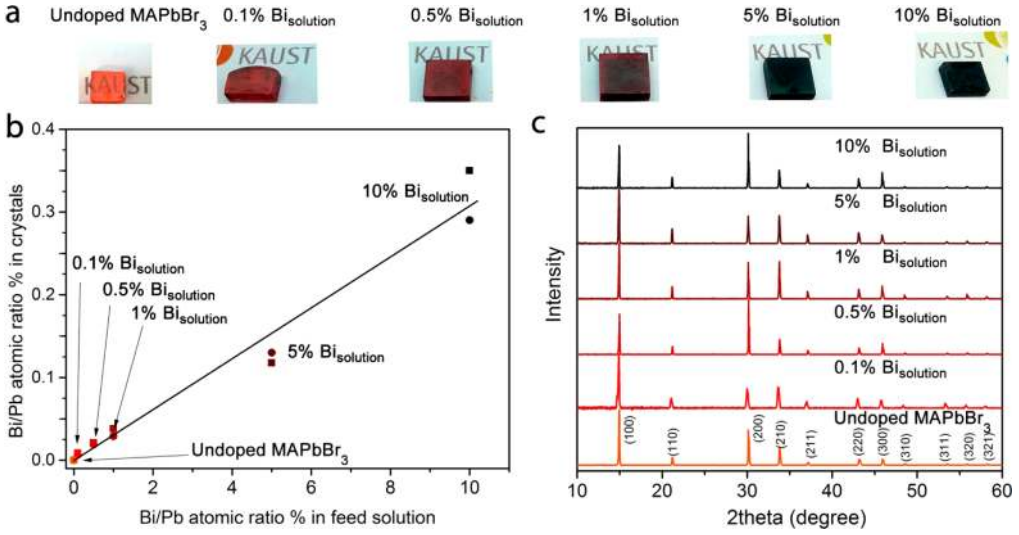

Figure 2. (a) Photographs showing $MAPbBr_3$ crystals having various Bi incorporation levels. (b) ICP measurement for Bi/Pb atomic ratio % as a function of feed solution atomic ratio %. (c) Powder XRD of ground $MAPbBr_3$ crystals with various Bi% doping.

dopant/Pb atomic ratio % was determined to be 0.029%, 0.020%, and 0.004% for Bi^{3+}, Au^{3+}, and In^{3+}, respectively. The Au^{3+} content measured by ICP indicates successful incorporation of the Au ions. Low In^{3+} content could be due to the large difference in ionic radii between lead and indium.[32] X-ray diffraction (XRD) patterns of powders made by grinding each type of crystal showed no extra peaks compared to the undoped crystal, indicating a single-phase material (Figure 1a) that retains the structural framework of pure $MAPbBr_3$ crystals. The preservation of the host perovskite structure, especially the inorganic framework, is important since this substructure is associated with the semiconducting properties of the organic–inorganic hybrids.[33]

As evidenced from the color of the crystals, the absorption edge of the Bi-doped crystal was red-shifted, while Au- and In-doped crystals showed no obvious spectral change from the undoped crystal (Figure 1b). This is consistent with prior reports that BGN is dependent on the nature of the dopant.[6] The BGN observed only in the case of Bi-doped crystals is in agreement with theoretical studies suggesting that the outer ns^2 electrons play a critical role in bandgap modulation.[34] Our density functional theory (DFT) calculations show that Au and In create deeper, more localized, and less interacting states than Bi, consistent with the failure of Au and In incorporation to produce notable BGN (Figure S3, Supporting Information).

The trivalent bismuth cation and Pb^{2+} have very similar ionic radii and are isoelectronic ($6s^2$), and this may explain the similarities in chemical behavior for these cations.[32] Previous reports have found that the bismuth cation forms regular chains built of nearly regular octahedra with halide anions;[35,36] in particular, the Bi–Br bond length[35] (axial: 2.926, equatorial: 2.849 and 2.826 Å) in the octahedron $BiBr_6^{3-}$ closely matches that of the Pb–Br bond (2.95 Å)[26] in the corresponding octahedral structure. Mitzi reported bismuth perovskites, yet with a distorted octahedral coordination leading to a lower-dimensionality material.[37] The degree of distortion of an octahedron in hybrid perovskites is dependent on the size of the organic cation, the inorganic cation, and the halide.[14] In addition, bismuth has been previously used to dope PbS in both thin films[38] and quantum dots,[39] converting them from p-type to n-type semiconductors. The lattice mismatch between PbS[39] and $MAPbBr_3$[28] is less than 1%, which may suggest Bi^{3+} could be incorporated into the bromide-based perovskites crystal as well.

Motivated by this remarkable resemblance of Bi and Pb, as well as our findings of effective incorporation—BGN and preservation of the lattice structure of the perovskite—we further explored the effect of bismuth concentration on crystal optoelectronic properties. The color of the crystal was readily tuned by controlling the concentration of Bi^{3+} in the feed solution, as seen in Figure 2a. The Bi content in the obtained crystals, identified using ICP-OES, was found to be substantially lower than the nominal precursor amount in the feed solution. However, the Bi content obtained by ICP still indicates a moderate-to-heavy doping regime.[40] Table 1 shows the Bi and Pb percentages in both the feed solution and the obtained crystals. Hereafter, for simplicity, we refer to the crystals by the Bi% in the feed solution. Figure 2b shows the measured Bi/Pb atomic ratio % as a function of Bi/Pb atomic ratio % in the feed solution. The reduction in the Pb% (Table 1) is not fully compensated by an equal increase in the Bi%, and this could be indicating the formation of Pb vacancies. Previous works reported that, in doped materials, the structure stabilizes through the formation of vacancies.[41,42] Our DFT studies (Figure S4, Supporting Information) indicate that Pb vacancies may also contribute to BGN. Although the position of the Bi atoms in the structure was not determined, the decrease in Pb content and the similarity in the ionic radii might suggest substitutional doping, and this is also consistent with our DFT calculations (Figure S5, Supporting Information). Figure 2c

Table 1. Bi and Pb Atomic % in the Feed Solution and Obtained Crystals

Bi% in feed solution	Bi%	Pb%	~number of Bi atoms per cm^3 of crystal
0 (undoped)	–	42.7 ± 0.7	–
0.1	0.0026 ± 0.0005	40.6 ± 0.7	4×10^{17}
0.5	0.0072 ± 0.0007	41.1 ± 0.7	1×10^{18}
1	0.0120 ± 0.0006	41.5 ± 0.7	2×10^{18}
5	0.055 ± 0.016	38.3 ± 0.6	6×10^{18}
10	0.120 ± 0.038	37.5 ± 0.6	2×10^{19}

DOI: 10.1021/acs.jpclett.5b02681
J. Phys. Chem. Lett. 2016, 7, 295–301

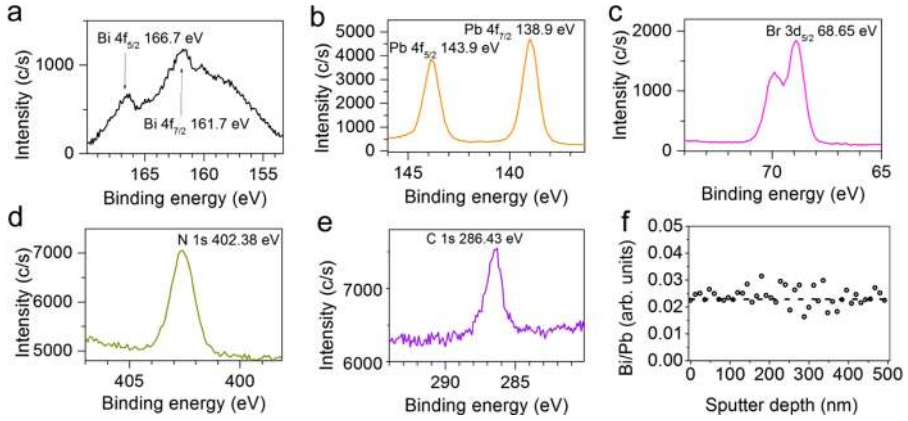

Figure 3. High-resolution XPS spectra of (a) Bi 4f, (b) Pb 4f, (c) Br 3d, (d) N 1s, (e) C 1s after single sputtering cycle and (f) sputter depth profile for the Bi/Pb ratio. A 500 eV Ar-ion beam was used for 2 min in a single sputtering cycle.

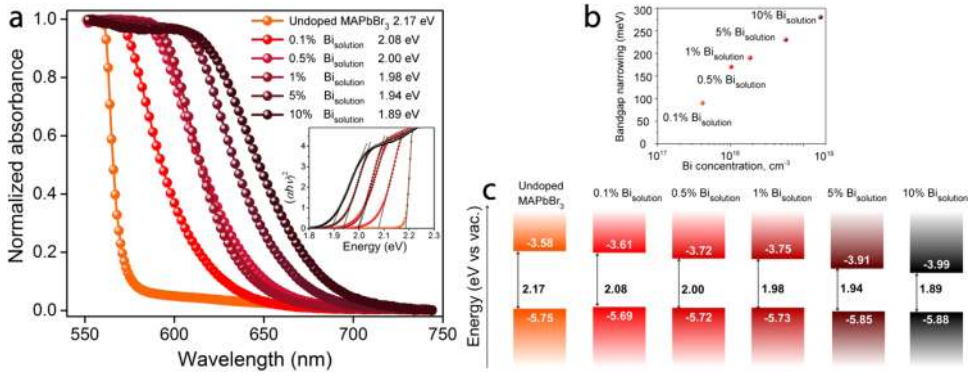

Figure 4. (a) Steady-state absorption spectra of $MAPbBr_3$ crystals with various Bi%. Inset: corresponding Tauc plots. (b) Bandgap narrowing as a function of Bi concentration in the crystal. (c) Bandgap alignment of $MAPbBr_3$ crystals with various Bi%.

shows XRD patterns of undoped and Bi-doped $MAPbBr_3$ crystals. Even at the highest doping level, the XRD pattern confirmed a single phase of the host cubic perovskite structure. Careful XRD analysis revealed no differences between the lattice parameters (5.92 Å) in both doped and undoped crystals. Similarly, there is no change in the full width at half maxima before and after doping (Table 1, Supporting Information).

Next, we inserted a number of freshly cleaved crystal surfaces with different Bi doping levels into an X-ray photoelectron spectroscopy (XPS) chamber and, following a single cycle of gentle sputtering, performed high-resolution XPS on each sample. The spectrometer dispersion was adjusted to give a binding energy of 284.8 eV for the C 1s line of adventitious (aliphatic) carbon presented on the non-sputtered samples (Figure S6, Supporting Information, and Table S2, Supporting Information). Figure 3 shows the representative high-resolution XPS spectra for the regions of interest of the most highly Bi-doped sample. The Bi 4f doublet is clearly resolved at the 161.7 eV (Bi $4f_{7/2}$) and 166.7 eV (Bi $4f_{5/2}$) binding energies (Figure 3a), slightly higher than the reported values for Bi^{3+} ions, which might suggest a different chemical environment.[43] The expected ratio of 4/3 for the spin−orbit split f-levels is in good agreement with the experimental data (Figure S7, Supporting Information and Table S3, Supporting Information). The Pb 4f doublet and Br 3d binding energies, shown in Figure 3b and 3c, respectively, are also slightly higher than the reported values for $MAPbBr_3$ thin films.[44] N 1s, and C 1s core level peaks are observed at 402.38 and 286.43 eV, respectively (Figure 3d,e, respectively). A possible explanation for the slightly higher binding energy values of Bi, Pb, and Br is that XPS measurements were conducted on bulk crystals rather than the commonly reported thin films. The sputtering regime we chose can be concluded to be a largely nondestructive, consistent with the stable surface chemical composition observed up to 500 nm in depth (see depth profiles in Figure 3f) of the crystal. The initial drop in carbon content and the increase in lead and bromine atomic concentrations can be attributed to the removal of surface contamination. This is supported by the significant reduction in the total carbon component due to its aliphatic component removal observed after the very first sputtering cycles. At the later stages, the intensity of the Bi and Pb signals remained essentially constant, indicating a uniform distribution of Bi, and also confirming the effectiveness of doping.

The normalized absorbance spectra of Bi-doped crystals exhibit a red-shift proportional to the Bi content (Figure 4a). The absolute absorbance spectra of the crystals are provided in Figure S8, Supporting Information. Figure 4b shows the BGN as a function of Bi concentration in the crystal. Even a much lower Bi percentage in solution (0.01%) can result in BGN (Figure S9, Supporting Information). The band edge shifted from 570 nm for the undoped crystal to 680 nm in the case of the highest Bi%. This latter corresponds to a bandgap value of 1.89 eV. BGN in doped semiconductors is caused by the interaction of the electrons with positive impurities, altering the density of states.[6,7] BGN may also be explained by the higher electronegativity of Bi compared to Pb, leading to more

DOI: 10.1021/acs.jpclett.5b02681
J. Phys. Chem. Lett. 2016, 7, 295−301

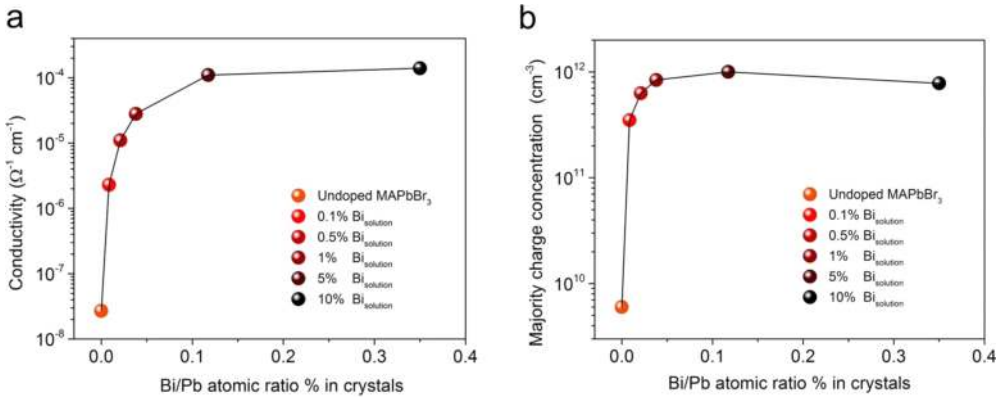

Figure 5. (a) Conductivity and (b) majority charge concentration of the different crystals as a function of Bi/Pb atomic ratio % in the crystals.

covalent bonding with bromide. This is consonant with the previously reported decrease in bandgap from Pb to Sn and Ge perovskites due to the difference in their electronegativity.[14] The relatively shallow (in comparison to Au and In) and delocalized Bi states, as determined using DFT, facilitate the mutual interaction of nearby Bi dopants—a condition required for bandgap narrowing (Figure S10, Supporting Information). We note that the band edge is not as sharp as in the undoped crystal, with tail states in the absorption. Such Urbach tails have been exploited in other doped semiconductors for nonlinear optical switching.[7] Notable bandtailing was also observed in mixed I/Br perovskite films;[45] nevertheless, they have been used successfully in optoelectronic devices.[46] It is worth mentioning that incorporating Bi^{3+} into the perovskite crystal quenches the photoluminescence, which is similar to what is observed in Bi-doped PbS quantum dots[39] and other doped quantum dots systems[47] and could be attributed to carrier capture into Bi-related energy band which is optically inactive.

Generally, time-resolved laser spectroscopy provides direct information about the carrier dynamics in organic and semiconductor materials.[48−50] In this study, nanosecond time-resolved transient absorption experiments reveal an extended carrier lifetime in crystals following Bi^{3+} incorporation. In addition to two time constants of tens and hundreds of nanoseconds (these are commonly observed for the undoped single crystals[26,28]), a new component with a characteristic time constant of several tens to hundreds of microseconds is observed for Bi-doped $MAPbBr_3$ crystals. The contribution of this component increases as the doping concentration (Figure S11, Supporting Information). Reduced recombination rates and longer lifetimes has been previously reported for mixed halide perovskites.[51]

The band positions of crystals were identified by combination of Photoelectron spectroscopy in air (PESA) and optical bandgap.[52] PESA was used to obtain the valence band maximum (VBM) from the onset energy value of the spectra (Figure S12, Supporting Information). Using the optical bandgaps (E_g), we deduced the conduction band minimum (CBM) from the relationship VBM + E_g = CBM, as previously reported by McGehee et al.[52] Figure 4c shows the values calculated for VBM and CBM. The conduction band moves downward considerably in energy, hinting that Bi doping may be prone to produce n-type semiconductors.

The sizable dimensions of the crystals synthesized using DIRR enabled the deposition of ohmic contacts for the study of electronic parameters such as conductivity (σ) and charge concentration (n) (Figure S13, Supporting Information, 10% Bi as an example). The four point probe method allows measurement of conductivity in semiconductor materials.[53] Using this method, we observed an increase in conductivity of as much as 4 orders of magnitude, from $\sim 10^{-8}$ Ω^{-1} cm^{-1} for the undoped crystal to $\sim 10^{-4}$ Ω^{-1} cm^{-1} for the highest-conductivity Bi-doped crystals (Figure 5a). As in Bi-doped PbS thin films reported previously,[38] a rapid and abrupt increase in conductivity is first observed, followed by a gradual saturation as higher dopant concentrations are approached.

Hall Effect studies revealed that free carrier concentration within Bi-doped crystals increases to $\sim 10^{11}$-10^{12} cm^{-3} compared to $\sim 10^{9}$ cm^{-3} for undoped crystals (Figure 5b). This indicates that, of the $\sim 10^{19}$ cm^{-3} impurity atoms introduced, only a certain fraction contribute free carriers.

$MAPbBr_3$ is an intrinsic p-type semiconductor.[26] Through Hall Effect measurements (Figure S13, Supporting Information), we were able to demonstrate the change in the sign of majority carriers from p- to n-type through converting the intrinsic perovskite semiconductor to an extrinsic one, which is in line with values obtained from simple semiconductor physics considerations (Note 1, Supporting Information). The change in the sign of charge carriers is in agreement with our measurements of VBM and CBM discussed earlier. This switching in behavior from p- to n-type has been reported for the Bi-doping of other materials systems such as PbS thin films[38] and quantum dots.[39] The mobility of charge carriers was coarsely estimated from $\mu = en/\sigma$ (e is the electron charge) to be an order of magnitude larger in doped compared to in undoped crystals. Although such an increase was previously observed in prior studies of certain materials systems,[54] it is usually the case that mobility decreases when high concentrations of impurities are introduced to the semiconductor.

Bandgap tailoring is clearly of interest across the family of hybrid perovskites, including in $MAPbI_3$. Although Bi-doped $MAPbBr_3$ crystals were used for many of the key studies herein, Bi-doped $MAPbI_3$ crystals also show a single phase material (Figure S14, Supporting Information) with BGN that depends systematically on the Bi%. The bandgap of $MAPbI_3$ is reduced from its intrinsic value of 1.51 eV[28] to as low as 1.28 eV (Figures S15 and S16, Supporting Information and Table 4, Supporting Information), a value of interest in photovoltaics.

In summary, we demonstrated herein an efficient in situ chemical route for the incorporation of heterovalent dopants into hybrid perovskite crystal through the DIRR technique. Trivalent metals such as Bi, Au, and In were successfully introduced while preserving the structure of the host perovskite. Our results suggest that Bi is a potential candidate

DOI: 10.1021/acs.jpclett.5b02681
J. Phys. Chem. Lett. 2016, 7, 295−301

for tuning a number of optical and electronic properties in the hybrid perovskite crystal. The performance of hybrid perovskite-based optoelectronic devices such as solar cells and photodetectors mainly rely on bandgap, conductivity, charge carrier concentration, and mobility of the semiconductor. The observed BGN upon doping, as well as the increase in the charge carrier concentration and conductivity, and notably the change in the majority charge carrier sign, suggest promise in a diverse set of perovskite-based optoelectronic devices.

■ ASSOCIATED CONTENT

Supporting Information

The Supporting Information is available free of charge on the ACS Publications website at DOI: 10.1021/acs.jpclett.5b02681.

Materials, synthesis, measurements, and characterization, along with the UV-photodetector setup (PDF)

■ AUTHOR INFORMATION

Corresponding Authors

*E-mail: osman.bakr@kaust.edu.sa.

*E-mail: omar.abdelsaboor@kaust.edu.sa.

Author Contributions

⊥(A.L.A., M.I.S.) These authors contributed equally to this work.

Notes

The authors declare no competing financial interest.

■ ACKNOWLEDGMENTS

The authors acknowledge the support of Awards URF/1/2268-01-01, URF/1/1741-01-01, and URF/1/1373-01-01 made by King Abdullah University of Science and Technology (KAUST). We acknowledge the financial support from King Abdulaziz City for Science and Technology (KACST), Grant KACST TIC R2-FP-008. The authors thank Y. Losovyj for XPS data collection and partial analysis, and P. Dowben for the useful discussions. Access to XPS at the Nanoscience Characterization Facility of Indiana University's Nanoscience Center was provided by the NSF (Award DMR MRI-1126394).

■ REFERENCES

(1) Abram, R. A.; Rees, G. J.; Wilson, B. L. H. Heavily Doped Semiconductors and Devices. *Adv. Phys.* **1978**, *27*, 799−892.

(2) Piao, Y.; Meany, B.; Powell, L. R.; Valley, N.; Kwon, H.; Schatz, G. C.; Wang, Y. Brightening of Carbon Nanotube Photoluminescence through the Incorporation of sp^3 Defects. *Nat. Chem.* **2013**, *5*, 840−845.

(3) Ehli, C.; Oelsner, C.; Guldi, D. M.; Mateo-Alonso, A.; Prato, M.; Schmidt, C.; Backes, C.; Hauke, F.; Hirsch, A. Manipulating Single-wall Carbon Nanotubes by Chemical Doping and Charge Transfer with Perylene Dyes. *Nat. Chem.* **2009**, *1*, 243−249.

(4) Khan, A.; Das, A. Diffusivity−Mobility Relationship for Heavily Doped Semiconductors Exhibiting Band Tails. *Phys. B* **2010**, *405*, 817−821.

(5) Berggren, K. F.; Sernelius, B. E. Band-Gap Narrowing in Heavily Doped Many-Valley Semiconductors. *Phys. Rev. B: Condens. Matter Mater. Phys.* **1981**, *24*, 1971−1986.

(6) Palankovski, V.; Kaiblinger-Grujin, G.; Selberherr, S. Study of Dopant-Dependent Band Gap Narrowing in Compound Semiconductor Devices. *Mater. Sci. Eng., B* **1999**, *66*, 46−49.

(7) Van Mieghem, P. Theory of Band Tails in Heavily Doped Semiconductors. *Rev. Mod. Phys.* **1992**, *64*, 755−793.

(8) Liebler, J.; Haug, H. Theory of the Band-Tail Absorption Saturation in Polar Semiconductors. *Phys. Rev. B: Condens. Matter Mater. Phys.* **1990**, *41*, 5843−5856.

(9) Maculan, G.; Sheikh, A. D.; Abdelhady, A. L.; Saidaminov, M. I.; Haque, M. A.; Murali, B.; Alarousu, E.; Mohammed, O. F.; Wu, T.; Bakr, O. M. $CH_3NH_3PbCl_3$ Single Crystals: Inverse Temperature Crystallization and Visible-Blind UV-Photodetector. *J. Phys. Chem. Lett.* **2015**, *6*, 3781−3786.

(10) Jung, H. S.; Park, N.-G. Perovskite Solar Cells: From Materials to Devices. *Small* **2015**, *11*, 10−25.

(11) Gonzalez-Pedro, V.; Juarez-Perez, E. J.; Arsyad, W.-S.; Barea, E. M.; Fabregat-Santiago, F.; Mora-Sero, I.; Bisquert, J. General Working Principles of $CH_3NH_3PbX_3$ Perovskite Solar Cells. *Nano Lett.* **2014**, *14*, 888−893.

(12) Chen, Y.-S.; Manser, J. S.; Kamat, P. V. All Solution-Processed Lead Halide Perovskite-$BiVO_4$ Tandem Assembly for Photolytic Solar Fuels Production. *J. Am. Chem. Soc.* **2015**, *137*, 974−981.

(13) Boix, P. P.; Agarwala, S.; Koh, T. M.; Mathews, N.; Mhaisalkar, S. G. Perovskite Solar Cells: Beyond Methylammonium Lead Iodide. *J. Phys. Chem. Lett.* **2015**, *6*, 898−907.

(14) Gao, P.; Gratzel, M.; Nazeeruddin, M. K. Organohalide Lead Perovskites for Photovoltaic Applications. *Energy Environ. Sci.* **2014**, *7*, 2448−2463.

(15) Saidaminov, M. I.; Adinolfi, V.; Comin, R.; Abdelhady, A. L.; Peng, W.; Dursun, I.; Yuan, M.; Hoogland, S.; Sargent, E. D.; Bakr, O. M. Planar-Integrated Single-Crystalline Perovskite Photodetectors. *Nat. Commun.* **2015**, *6*, 8724.

(16) Nie, W.; Tsai, H.; Asadpour, R.; Blancon, J.-C.; Neukirch, A. J.; Gupta, G.; Crochet, J. J.; Chhowalla, M.; Tretiak, S.; Alam, M. A.; et al. High-Efficiency Solution-Processed Perovskite Solar Cells With Millimeter-Scale Grains. *Science* **2015**, *347*, 522−525.

(17) Kojima, A.; Teshima, K.; Shirai, Y.; Miyasaka, T. Organometal Halide Perovskites as Visible-Light Sensitizers for Photovoltaic Cells. *J. Am. Chem. Soc.* **2009**, *131*, 6050−6051.

(18) Yang, W. S.; Noh, J. H.; Jeon, N. J.; Kim, Y. C.; Ryu, S.; Seo, J.; Seok, S. I. High-Performance Photovoltaic Perovskite Layers Fabricated through Intramolecular Exchange. *Science* **2015**, *348*, 1234−1237.

(19) Stranks, S. D.; Eperon, G. E.; Grancini, G.; Menelaou, C.; Alcocer, M. J. P.; Leijtens, T.; Herz, L. M.; Petrozza, A.; Snaith, H. J. Electron-Hole Diffusion Lengths Exceeding 1 Micrometer in an Organometal Trihalide Perovskite Absorber. *Science* **2013**, *342*, 341−344.

(20) Tidhar, Y.; Edri, E.; Weissman, H.; Zohar, D.; Hodes, G.; Cahen, D.; Rybtchinski, B.; Kirmayer, S. Crystallization of Methyl Ammonium Lead Halide Perovskites: Implications for Photovoltaic Applications. *J. Am. Chem. Soc.* **2014**, *136*, 13249−13256.

(21) de Quilettes, D. W.; Vorpahl, S. M.; Stranks, S. D.; Nagaoka, H.; Eperon, G. E.; Ziffer, M. E.; Snaith, H. J.; Ginger, D. S. Impact of Microstructure on Local Carrier Lifetime in Perovskite Solar Cells. *Science* **2015**, *348*, 683−686.

(22) Colella, S.; Mosconi, E.; Fedeli, P.; Listorti, A.; Gazza, F.; Orlandi, F.; Ferro, P.; Besagni, T.; Rizzo, A.; Calestani, G.; et al. R. $MAPbI_{(3-x)}Cl_x$ Mixed Halide Perovskite for Hybrid Solar Cells: the Role of Chloride as Dopant on the Transport and Structural Properties. *Chem. Mater.* **2013**, *25*, 4613−4618.

(23) Navas, J.; Sánchez-Coronilla, A.; Gallardo, J. J.; Cruz Hernández, N.; Piñero, J. C.; Alcántara, R.; Fernández-Lorenzo, C.; De los Santos, D. M.; Aguilar, T.; Martín-Calleja, J. New Insights into Organic-Inorganic Hybrid Perovskite $CH_3NH_3PbI_3$ Nanoparticles. An Experimental and Theoretical Study of Doping in Pb^{2+} Sites with Sn^{2+}, Sr^{2+}, Cd^{2+} and Ca^{2+}. *Nanoscale* **2015**, *7*, 6216−6229.

(24) Zhao, Y.; Zhu, K. Solution Chemistry Engineering toward High-Efficiency Perovskite Solar Cells. *J. Phys. Chem. Lett.* **2014**, *5*, 4175−4186.

(25) Eperon, G. E.; Burlakov, V. M.; Docampo, P.; Goriely, A.; Snaith, H. J. Morphological Control for High Performance, Solution-Processed Planar Heterojunction Perovskite Solar Cells. *Adv. Funct. Mater.* **2014**, *24*, 151−157.

(26) Shi, D.; Adinolfi, V.; Comin, R.; Yuan, M.; Alarousu, E.; Buin, A.; Chen, Y.; Hoogland, S.; Rothenberger, A.; Katsiev, K.; et al. Low

DOI: 10.1021/acs.jpclett.5b02681
J. Phys. Chem. Lett. 2016, 7, 295−301

Trap-State Density and Long Carrier Diffusion in Organolead Trihalide Perovskite Single Crystals. *Science* **2015**, *347*, 519−522.
(27) Stoumpos, C. C.; Malliakas, C. D.; Kanatzidis, M. G. Semiconducting Tin and Lead Iodide Perovskites with Organic Cations: Phase Transitions, High Mobilities, and Near-infrared Photoluminescent Properties. *Inorg. Chem.* **2013**, *52*, 9019−9038.
(28) Saidaminov, M. I.; Abdelhady, A. L.; Murali, B.; Alarousu, E.; Burlakov, V. M.; Peng, W.; Dursun, I.; Wang, L.; He, Y.; Maculan, G.; et al. High-Quality Bulk Hybrid Perovskite Single Crystals within Minutes by Inverse Temperature Crystallization. *Nat. Commun.* **2015**, *6*, 7586.
(29) Saidaminov, M. I.; Abdelhady, A. L.; Maculan, G.; Bakr, O. M. Retrograde Solubility of Formamidinium and Methylammonium Lead Halide Perovskites Enabling Rapid Single Crystal Growth. *Chem. Commun.* **2015**, *51*, 17658−17661.
(30) Li, C.; Lu, X.; Ding, W.; Feng, L.; Gao, Y.; Guo, Z. Formability of ABX_3 (X = F, Cl, Br, I) Halide Perovskites. *Acta Crystallogr., Sect. B: Struct. Sci.* **2008**, *64*, 702−707.
(31) Shockley, W.; Queisser, H. J. Detailed Balance Limit of Efficiency of p-n Junction Solar Cells. *J. Appl. Phys.* **1961**, *32*, 510.
(32) Shannon, R. Revised Effective Ionic Radii and Systematic Studies of Interatomic Distances in Halides and Chalcogenides. *Acta Crystallogr., Sect. A: Cryst. Phys., Diffr., Theor. Gen. Crystallogr.* **1976**, *32*, 751−767.
(33) Bi, W.; Louvain, N.; Mercier, N.; Luc, J.; Rau, I.; Kajzar, F.; Sahraoui, B. A Switchable NLO Organic-Inorganic Compound based on Conformationally Chiral Disulfide Molecules and $Bi(III)I_5$ Iodobismuthate Networks. *Adv. Mater.* **2008**, *20*, 1013−1017.
(34) Wang, K.; Liang, Z.; Wang, X.; Cui, X. Lead Replacement in $CH_3NH_3PbI_3$ Perovskites. *Adv. Electron. Mater.* **2015**, *1*, 1500089.
(35) Bi, W.; Leblanc, N.; Mercier, N.; Auban-Senzier, P.; Pasquier, C. Thermally Induced Bi(III) Lone Pair Stereoactivity: Ferroelectric Phase Transition and Semiconducting Properties of $(MV)BiBr_5$ (MV = methylviologen). *Chem. Mater.* **2009**, *21*, 4099−4101.
(36) Leblanc, N.; Mercier, N.; Zorina, L.; Simonov, S.; Auban-Senzier, P.; Pasquier, C. Large Spontaneous Polarization and Clear Hysteresis Loop of a Room-Temperature Hybrid Ferroelectric Based on Mixed-Halide $[BiI_3Cl_2]$ Polar Chains and Methylviologen Dication. *J. Am. Chem. Soc.* **2011**, *133*, 14924−14927.
(37) Mitzi, D. B. Organic−Inorganic Perovskites Containing Trivalent Metal Halide Layers: the Templating Influence of the Organic Cation Layer. *Inorg. Chem.* **2000**, *39*, 6107−6113.
(38) Abe, S.; Masumoto, K.; Suto, K. Growth and Characterization of Bi-doped PbS Thin Films Prepared by Hot-Wall Epitaxy. *J. Cryst. Growth* **1997**, *181*, 367−373.
(39) Stavrinadis, A.; Rath, A. K.; de Arquer, F. P. G.; Diedenhofen, S. L.; Magén, C.; Martinez, L.; So, D.; Konstantatos, G. Heterovalent Cation Substitutional Doping for Quantum Dot Homojunction Solar Cells. *Nat. Commun.* **2013**, *4*, 2981.
(40) Achuthan, M. A.; Bhat, K. N. *Fundamentals of Semiconductor Devices*; Tata McGraw-Hill Education: New Delhi, 2006.
(41) Zunger, A. Practical Doping Principles. *Appl. Phys. Lett.* **2003**, *83*, 57−59.
(42) Neagu, D.; Tsekouras, G.; Miller, D. N.; Ménard, H.; Irvine, J. T. S. In situ Growth of Nanoparticles through Control of Non-stoichiometry. *Nat. Chem.* **2013**, *5*, 916−923.
(43) Liu, H.; Nakamura, R.; Nakato, Y. Promoted Photo-Oxidation Reactivity of Particulate $BiVO_4$ Photocatalyst Prepared by a Photo-assisted Sol-Gel Method. *J. Electrochem. Soc.* **2005**, *152*, G856−G861.
(44) Kim, Y.-H.; Cho, H.; Heo, J. H.; Kim, T.-S.; Myoung, N.; Lee, C.-L.; Im, S. H.; Lee, T.-W. Multicolored Organic/Inorganic Hybrid Perovskite Light-Emitting Diodes. *Adv. Mater.* **2015**, *27*, 1248−1254.
(45) Fedeli, P.; Gazza, F.; Calestani, D.; Ferro, P.; Besagni, T.; Zappettini, A.; Calestani, G.; Marchi, E.; Ceroni, P.; Mosca, R. Influence of the Synthetic Procedures on the Structural and Optical Properties of Mixed-Halide (Br, I) Perovskite Films. *J. Phys. Chem. C* **2015**, *119*, 21304−21313.
(46) Bi, C.; Yuan, Y.; Fang, Y.; Huang, J. Perovskite Solar Cells: Low-Temperature Fabrication of Efficient Wide-Bandgap Organolead Trihalide Perovskite Solar Cells. *Adv. Energy Mater.* **2015**, *5*, 1401616.
(47) Jana, S.; Srivastava, B. B.; Jana, S.; Bose, R.; Pradhan, N. Multifunctional Doped Semiconductor Nanocrystals. *J. Phys. Chem. Lett.* **2012**, *3*, 2535−2540.
(48) Pan, J.; Sarmah, S. P.; Murali, B.; Dursun, I.; Peng, W.; Parida, M. R.; Liu, J.; Sinatra, L.; Alyami, N.; Zhao, C.; et al. Air-Stable Surface-Passivated Perovskite Quantum Dots for Ultra-Robust, Single- and Two-Photon-Induced Amplified Spontaneous Emission. *J. Phys. Chem. Lett.* **2015**, *6*, 5027−5033.
(49) Aly, S. M.; Parida, M. R.; Alarousu, E.; Mohammed, O. F. Ultrafast Electron Injection at the Cationic Porphyrin−Graphene Interface Assisted by Molecular Flattening. *Chem. Commun.* **2014**, *50*, 10452−10455.
(50) Bose, R.; Ahmed, G. H.; Alarousu, E.; Parida, M. R.; Abdelhady, A. L.; Bakr, O. M.; Mohammed, O. F. Direct Femtosecond Observation of Charge Carrier Recombination in Ternary Semiconductor Nanocrystals: the Effect of Composition and Shelling. *J. Phys. Chem. C* **2015**, *119*, 3439−3446.
(51) Suarez, B.; Gonzalez-Pedro, V.; Ripolles, T. S.; Sanchez, R. S.; Otero, L.; Mora-Sero, I. Recombination Study of Combined Halides (Cl, Br, I) Perovskite Solar Cells. *J. Phys. Chem. Lett.* **2014**, *5*, 1628−1635.
(52) Nguyen, W. H.; Bailie, C. D.; Unger, E. L.; McGehee, M. D. Enhancing the Hole-Conductivity of Spiro-OMeTAD without Oxygen or Lithium Salts by Using $Spiro(TFSI)_2$ in Perovskite and Dye Sensitized Solar Cells. *J. Am. Chem. Soc.* **2014**, *136*, 10996−11001.
(53) Li, J. C.; Wang, Y.; Ba, D. C. Characterization of Semiconductor Surface Conductivity by Using Microscopic Four-Point Probe Technique. *Phys. Procedia* **2012**, *32*, 347−355.
(54) Dakhel, A. A. Improving Carriers Mobility in Copper and Iron-Codoped CdO. *Mater. Sci. Semicond. Process.* **2014**, *17*, 194−198.

DOI: 10.1021/acs.jpclett.5b02681
J. Phys. Chem. Lett. 2016, 7, 295−301